W' production at the LHC in the 4-site Higgsless model

Elena Accomando* and Diego Becciolini†

NExT Institute and School of Physics and Astronomy,

University of Southampton, Highfield, Southampton SO17 1BJ, UK

Stefania De Curtis‡

Istituto Nazionale di Fisica Nucleare, Sezione di Firenze -Italy

Daniele Dominici§ and Luca Fedeli¶

Università degli Studi di Firenze, Dip. di Fisica e Astronomia, Firenze - Italy

and Istituto Nazionale di Fisica Nucleare, Sezione di Firenze - Italy

(Dated: September 7, 2011)

We study the phenomenology of the 4-site Higgsless model, based on the $SU(2)_L \times SU(2)_1 \times SU(2)_2 \times U(1)_Y$ gauge symmetry, at present colliders. The model predicts the existence of two neutral and four charged extra gauge bosons, $Z_{1,2}$ and $W^{\pm}_{1,2}$. In this paper, we focus on the charged gauge sector. We first derive limits on $W_{1,2}$-boson masses and couplings to SM fermions from direct searches at the Tevatron. We then estimate at the 7 TeV LHC the exclusion limits with the actual L=1 fb^{-1} and the discovery potential with the expected L=10 fb^{-1}. In contrast to the minimal (or 3-site) Higgsless model which predicts almost fermiophobic extra gauge bosons, the next-to-minimal (or 4-site) Higgsless model recovers sizeable $W_{1,2}$-boson couplings to ordinary matter, expressing the non-fermiophobic multiresonance inner nature of extra-dimensional theories. Owing to this feature, we find that in one year from now the new heavy gauge bosons, $W^{\pm}_{1,2}$, could be discovered in the final state with an electron and large missing transverse energy at the 7 TeV LHC for $W_{1,2}$-boson masses in the TeV region, depending on model parameters.

PACS numbers: 12.60.Cn, 11.25.Mj, 12.39.Fe

I. INTRODUCTION

Extra gauge bosons W' are predicted in many models that extend the gauge structure of the Standard Model (SM). Left-Right symmetric models [1, 2, 3], based on the enlarged symmetry $SU(2)_L \otimes SU(2)_R \otimes U(1)$, are an old and popular example; the discovery reach and the study of W' properties at the LHC has been recently re-investigated [4, 5, 6] and bounds from early LHC data have been derived [7]. Heavy charged gauge bosons are also a natural consequence of Minimal Walking Technicolor (MWT) models. For a complete review see Refs.[8, 9] and references therein. The LHC potential of detecting such particles have been extensively analysed [10, 11].

During the last ten years, the idea of extra dimensions [12, 13, 14] has been very fruitful in the proposal of extensions of the SM with or without the Higgs [15, 16, 17, 18, 19, 20, 21, 22]. In these models, the W' bosons emerge as Kaluza Klein excitations of the SM W-boson. The possibility to discover them at the LHC has been investigated many years ago [23]. Recently, a more refined analysis has been performed [24]. New peculiar LHC signals from extra charged and neutral gauge bosons have been also studied within the RS1 models with gauge bosons in the five-dimensional bulk and fermions on the UV brane (except for the third generation quark) [25, 26]. In these models EWPT (Electroweak Precision Tests) favor masses of the order of 2-3 TeV and therefore integrated luminosity of order 100 fb^{-1} are required to observe the lightest states in final state top-bottom quark pairs.

The five-dimensional models can also be deconstructed to the usual four-dimensional space-time [27, 28, 29, 30, 31, 32, 33, 34, 35], where they are described by a class of chiral Lagrangians with extended gauge symmetries. Within the simplest deconstructed models (e.g. the 3-site model), the consistency of the $\epsilon_3(S)$ parameter with its experimental value is satisfied at tree level via the ideal localization of fermions [36, 37, 38, 39, 40]. This makes the additional gauge bosons almost fermiophobic. As a consequence, the literature is mainly focused on complicated production channels: vector boson associated production

*Electronic address: E.Accomando@soton.ac.uk
†Electronic address: diego.becciolini@soton.ac.uk
‡Electronic address: decurtis@fi.infn.it
§Electronic address: dominici@fi.infn.it
¶Electronic address: fedeli@fi.infn.it

and vector boson fusion. All these processes require high luminosity and high energy to be detected [41, 42, 43]. The inclusion of one-loop corrections to the $\epsilon_3(S)$ parameter allows for non vanishing couplings of the new gauge bosons to SM fermions [44]. In this case, the Drell-Yan (DY) production channel opens up. And, if followed by the most promising W' decay into WZ-pairs, it could allow to detect the new heavy gauge bosons at the 14 TeV LHC with less than 10 fb^{-1} [45, 46].

The 4-site extension is instead much less bounded. The relation between the couplings of the two new gauge boson triplets with SM fermions is indeed strongly constrained by the ϵ_3-parameter, but their magnitude is weakly limited by ϵ_1 [47, 48]. The phenomenological consequence is that, while the minimal 3-site Higgsless model can be explored only in complex multi-particle processes (the easiest one being $pp \to VV \to 4f$ with $V = W, Z$), the 4-site Higgsless model can be tested in the more promising Drell-Yan channel with lepton pairs in the final state [47, 49].

This paper is devoted to a detailed study of signal and background for the leptonic Drell-Yan production of the two new charged gauge bosons predicted by the 4-site Higgsless model [47, 49, 50, 51, 52]. A similar analysis was recently performed within the Minimal Walking Technicolor [10, 11]. Compared to the latter, the 4-site model differs by the nature of the two extra gauge bosons: the lighter is at leading order a vector particle while the heavier is an axial particle. The mass splitting $M_{W2} - M_{W1}$ is always positive and, oppositely to the Minimal Walking Technicolor, no mass spectrum inversion is possible. In the following, we consider final states with one isolated electron and large missing transverse momentum. We plan to investigate the $pp \to W' \to WZ \to 4f$ mode in the future. In some cases, the latter channel is the most favorable for the observation of a heavy vector boson. Clearly, this is true when the bosonic decay modes are larger and consequently the already small branching ratios (BR) for the leptonic modes are further suppressed. In some models the leptonic modes could even be forbidden or very strongly suppressed as already noticed [53, 54, 55, 56].

The W' boson has been recently searched at the Tevatron and the LHC in different final states. We make use of the leptonic DY channel analysis [57, 58, 59, 60] to extract limits on the parameter space of the 4-site model and explore the discovery reach in the near future.

In Sections II and III, we review the 4-site model and the properties of the two new charged gauge bosons. Section IV is devoted to investigate the DY production at the LHC and the Tevatron in the leptonic channel. In Section V, we present exclusion and discovery

reach and finally in Sect. VI we give our conclusions.

II. THE 4-SITE HIGGSLESS MODEL

The 4-site Higgsless model represents the next-to-minimal extension of the 3-site Higgsless model [61] that corresponds to a particular choice of the BESS model [62, 63]. They both belong to the class of deconstructed Higgsless theories [27, 28, 29, 30, 31, 32, 33, 34, 35]. In their general formulation, these theories are based on the $SU(2)_L \otimes SU(2)^K \otimes U(1)_Y$ gauge symmetry, and contain K+1 non-linear σ-model scalar fields interacting with the gauge fields, which trigger the spontaneous electroweak symmetry breaking. They constitute a viable alternative to the standard EWSB mechanism based on the existence of a light fundamental Higgs boson. The case K=1 corresponds to the minimal Higgsless model, more commonly called 3-site model.

The 4-site Higgsless model is defined by taking K=2, and requiring the Left-Right (LR) symmetry in the gauge sector. More explicitly, it is a linear moose based on the electroweak gauge symmetry $SU(2)_L \otimes SU(2)_1 \otimes SU(2)_2 \otimes U(1)_Y$. Its theoretical foundations are presented in [36], while some of its phenomenological consequences are analyzed in [47, 48, 49, 50].

In the unitary gauge, the 4-site model predicts two new triplets of gauge bosons, which acquire mass through the same non-linear symmetry breaking mechanism giving mass to the SM gauge bosons. Let us denote with $W^{\pm}_{i\mu}$ and $Z_{i\mu}$ (i = 1, 2) the four charged and two neutral heavy resonances appearing as a consequence of the gauge group extension, and with $W^{\pm}_{\mu}$, Z_μ and A_μ the SM gauge bosons. Owing to its gauge structure, the 4-site Higgsless model a priory contains seven free parameters: the $SU(2)_L \otimes U(1)_Y$ gauge couplings, $\tilde{g}$ and $\tilde{g}'$, the extra $SU(2)_{1,2}$ gauge couplings that, for simplicity, we assume to be equal, $g_2 = g_1$, the bare masses of lighter $(W^{\pm}_1, Z_1)$ and heavier $(W^{\pm}_2, Z_2)$ gauge boson triplets, $M_{1,2}$, and their bare direct couplings to SM fermions, $b_{1,2}$. However, their number can be reduced to four, by fixing the gauge couplings $\tilde{g}, \tilde{g}', g_1$ in terms of the three SM input parameters e, G_F, M_Z which denote electric charge, Fermi constant and Z-boson mass, respectively. As a result, the parameter space is completely defined by four independent free parameters which we choose to be: M_1, z, b_1 and b_2, where $z = M_1/M_2$ is the ratio between the bare masses. In terms of these four parameters, physical masses and couplings of the extra gauge bosons to ordinary matter can be obtained via a complete numerical algorithm. This is one

of the main results of [48] where we have describe in full detail this computation, which goes beyond the approximations commonly adopted in the literature. The outcome is the ability to reliably and accurately describe the full parameter space of the 4-site Higgsless model even in regions of low mass and high z where previously used approximations would fail. In the following, we choose to describe the full parameter space via the physical observables: $M_{W1}, z, a_{W1}, a_{W2}$ which denote the mass of the lighter extra charged gauge boson, the ratio between bare masses (which, as shown in [48] is a good approximation of the ratio between physical masses M_{W1}/M_{W2}), and the couplings of lighter and heavier extra charged gauge bosons to ordinary matter, respectively.

In terms of the above quantities, the Lagrangian describing the interaction between gauge bosons and fermions has the following expression:

$$\begin{aligned} \mathcal{L}_{NC} &= \bar{\psi}\gamma^{\mu}\left[-e\mathbf{Q}^{f}A_{\mu} + a_{Z}^{f}Z_{\mu} + a_{Z_1}^{f}Z_{1\mu} + a_{Z_2}^{f}Z_{2\mu}\right]\psi \\ \mathcal{L}_{CC} &= \bar{\psi}\gamma^{\mu}T^{-}\psi\left(a_{W}W_{\mu}^{+} + a_{W_1}W_{1\mu}^{+} + a_{W_2}W_{2\mu}^{+}\right) + h.c. \end{aligned} \tag{1}$$

for the neutral (NC) and charged (CC) gauge sector, respectively. In the above formulas, ψ denotes SM quarks and leptons. These expressions will be used later when discussing production and decay of the two extra charged gauge bosons in the Drell-Yan channel.

Before performing any meaningful analysis, it is mandatory to evaluate the impact of the Electroweak Precision Tests on the 4-site model. In the next section, we therefore review the constraints on the 4-site parameter space coming from EWPT.

A. EWPT bounds

Universal electroweak radiative corrections to the precision observables measured by LEP, SLD and TEVATRON experiments can be efficiently quantified in terms of three parameters: ϵ_1, ϵ_2, and ϵ_3 (or S, T, and U) [64, 65, 66, 67]. Besides these SM contributions, the ϵ_i (i=1,2,3) parameters allow to describe the low-energy effects of potential heavy new physics. For that reason, they are a powerful method to constrain theories beyond the SM. In a recent paper [48], we used this parametrization to extract bounds on the 3-site and 4-site Higgsless models. In order to derive realistic and reliable constraints, we performed a complete numerical calculation of all ϵ_i (i=1,2,3) parameters at tree level, going beyond popular approximations used in the past, and carried out a combined fit to the experimental results taking into

account their full correlation. The outcome represents a drastic update of past analysis. In the literature, in fact, these tree level new physics effects had been evaluated via an analytical truncated multiple expansion in the extra gauge coupling, e/g_1, and the direct couplings of the extra gauge bosons with SM fermions (or delocalization parameters), that is $b_{1,2}$ in our notation. The exact result we presented in [48] allows one to span the full parameter space of the model, reliably computing also regions characterized by small g_1 (or M_1) values, and sizeable $b_{1,2}$ bare couplings where the common approximated expansion would fail.

The major consequence of the analysis in [48] is that both ϵ_1 and ϵ_3 play a fundamental role in constraining the 4-site Higgsless model (ϵ_1 being usually considered sub-dominant). While ϵ_3 generates a strong correlation between the couplings of lighter and heavier extra charged (or neutral) gauge bosons to SM fermions, $a_{W1,W2}$, the ϵ_1 parameter limits indeed their magnitude. This effect is shown in the left panel of Fig. 1, where we plot the 95% CL limits from EWPT in the a_{W1}, a_{W2} plane for z=0.8 and two M_{W1} reference values. Let us notice that the signs of the physical fermion-boson couplings are completely arbitrary and physically irrelevant, what only matters is their size. We introduce signs to distinguish different points of the parameter space [48].

Owing to the above mentioned correlation, the number of free parameters can be further reduced to three. With this mild approximation, we can choose to describe the parameter space of the 4-site model in terms of the following set of physical quantities: M_{W1}, a_{W1} and z. The right panel of Fig. 1 displays the 95% CL bounds from EWPT in the M_{W1}, a_{W1} plane for four reference values of the z parameters: z=0.4, 0.6, 0.8 and 0.95. From Fig. 1 we deduce that, even if constrained, the a_{W1} coupling can be of the same order of magnitude than the corresponding SM coupling. This result is common to all other couplings between extra gauge bosons and ordinary matter, which can be uniquely derived from a_{W1} via our complete numerical algorithm. This is an important property which makes a very clear distinction between 4-site and 3-site model. The latter predicts indeed a unique gauge boson triplet, constrained to be (almost) fermiophobic in order to reconcile unitarity and EWPT bounds. This feature can be extrapolated from Fig. 1 by looking at the strong z-parameter dependence of the contours, which shrink with decreasing z, going towards the $z \to 0$ limit where one recovers the 3-site Higgsless model. Hence, oppositely to the minimal model, the next-to-minimal extension (or 4-site) displays the inner extra-dimensional nature

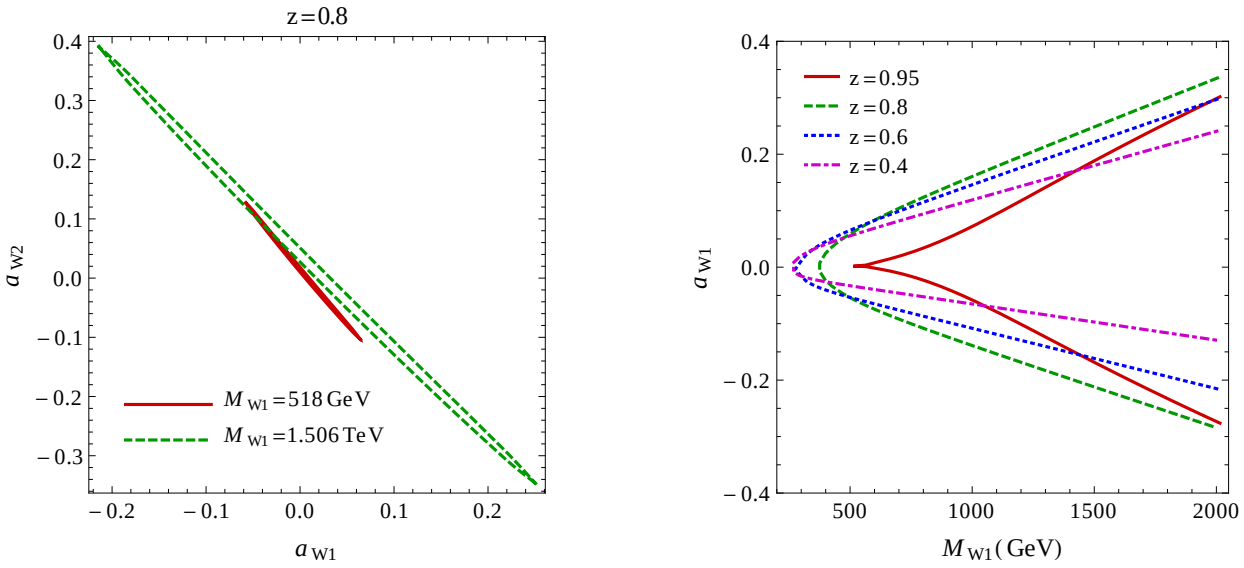

FIG. 1: Left: 95% CL limits from EWPT in the a_{W1}, a_{W2} plane for z=0.8 and two reference values of the lighter extra gauge boson mass, M_{W1}. Right: 95% CL EWPT bound in the parameter space given in terms of physical mass, M_{W1} , and physical coupling between lighter extra charged gauge bosons and SM fermions, a_{W1}. We consider four reference z-values: z= 0.4, 0.6, 0.8 and 0.95. The allowed regions are delimited by the curves.

of Higgsless theories, which are characterized by a tower of non-fermiophobic Kaluza-Klein resonances. The 4-site model has thus the potential of being detected during the early stage of the LHC experiment in the Drell-Yan channel.

An additional information, one can extract from the right panel of Fig. 1, concerns the minimum mass of the extra gauge bosons allowed by EWPT. As one can see, its value depends on the z free parameter and can range between 250 GeV and 600 GeV (see Ref.[48] for computational details). In this analysis we have not included the bounds on the trilinear gauge boson vertex, WWZ coming from the LEP2 experiment [68]. The maximum allowed value for the mass of the extra gauge bosons is instead fixed by the requirement of perturbative unitarity. As well known, one of the main motivations for Higgsless theories predicting an extended gauge sector, compared to the SM with no light elementary Higgs, is the ability to delay the perturbative unitarity violation up to energy scales of the order of a few TeV. Beyond that scale, new physics should come out. Higgsless theories must be indeed interpreted as effective low energy theories. In [47, 49, 50], all vector boson scattering

(VBS) amplitudes which are the best smoking gun for unitarity violations are computed, with the conclusion that the 4-site Higgsless model should preserve unitarity up to around 3 TeV. In the following, we assume this mass validity range.

III. EXTRA $W^{\pm}_{1,2}$-BOSONS: MASS SPECTRUM, DECAY WIDTHS AND BRANCHING RATIOS

In this section, we summarize the main properties of the heavy charged gauge bosons, $W^{\pm}_{1,2}$, predicted by the 4-site Higgsless model. A first peculiarity of the 4-site model is related to the nature of the four charged extra gauge bosons and their mass hierarchy. The two lighter particles, $W^{\pm}_1$, are vector bosons while the heavier ones, $W^{\pm}_2$, are axial-vectors (in a 5D sense, and neglecting electroweak corrections). Oppositely to closely related models, like the walking technicolor [11], no mass spectrum inversion is possible. The mass splitting, $\Delta M = M_{W2} - M_{W1}$, is always positive and its size depends on the free z-parameter:

$$\Delta M \sim \frac{1-z}{z} M_{W1} \qquad 0 < z < 1. \tag{2}$$

The above Eq. (2) contains also informations on the kind of multi-resonance spectrum we might expect. Owing to the z-parameter dependence, there is no fixed relation between the two charged gauge boson masses. We can thus have scenarios where the two charged resonances, $W^{\pm}_1$ and $W^{\pm}_2$, lie quite apart from each other, and portions of the parameter space in which they are (almost) degenerate. In the latter case, the multi-resonance distinctive signature would collapse into the more general single $W'^{\pm}$ signal. The 4-site model would thus manifest a degeneracy with well known theories predicting only one additional pair of charged gauge bosons. The mass spectrum has both a lower and an upper bound, as discussed in Sect.II A. It lies roughly in the range $250 \leq M(\mathrm{GeV}) \leq 3000$.

The total widths of the heavy charged gauge bosons divided by the corresponding mass, $\Gamma_{W1,W2}/M_{W1,W2}$, are displayed in Fig. 2 as a function of the mass for four representative values of the z-parameter: z=0.4, 0.6, 0.8, 0.95. They have been computed by taking as $W^{\pm}_{1,2} f f'$ couplings those corresponding to the maximum value of a_{W1} allowed by EWPT at fixed z-parameter (see contour plot in the right panel of Fig.1). This maximizes the fermionic contribution to the total decay width, and it will be used later to show the maximal branching ratio one might expect for the $W^{\pm}_{1,2}$-boson decay into electrons. From Fig. 2, one can see

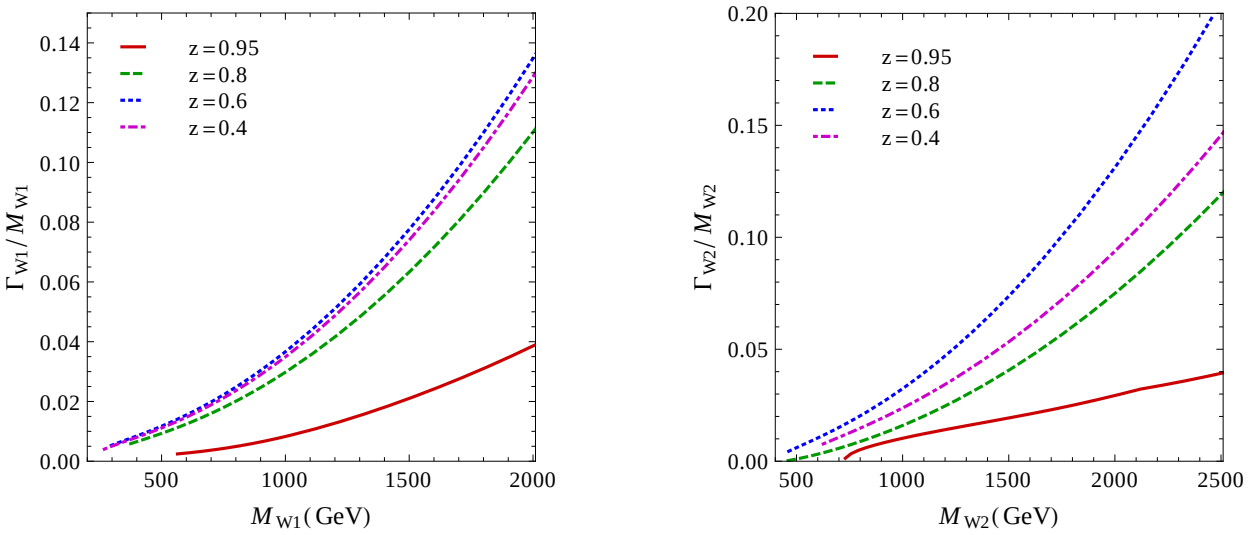

FIG. 2: Left: Total decay width of the lighter extra charged gauge boson, $W_1^{\pm}$, divided by its mass as a function of M_{W1} for four reference values of the z-parameter: z=0.4,0.6,0.8,0.95. Right: same for the heavier extra charged gauge boson, $W_2^{\pm}$.

that both $W_{1,2}^{\pm}$ are very narrow for low mass values. In the low edge of the spectrum, the magnitude of the $W_1^{\pm}$-boson total width is around a few GeV as shown in the left panel. For the $W_2^{\pm}$-boson in the right panel, it can go even down to a few MeV. The width is dominated by the $W_{1,2}^{\pm}$-boson decay into gauge boson pairs (when kinematically allowed) whose behaviors is proportional to $M_{W1,W2}^3$, it then increases with the mass up to hundreds of GeV. Since the $W_{1,2}^{\pm}$-boson total width can range between a few and hundreds of GeV, a natural question is whether one can still apply the ordinary experimental analysis based on the assumption of narrow resonances. In the 4-site model indeed, both ratios $\Gamma_{W1,W2}/M_{W1,W2}$ can be bigger than the SM one, $\Gamma_W/M_W \simeq 2.6\%$, already for relatively low masses $M_{W1} \simeq$ 800 GeV, and they can approach higher values up to about $\Gamma_{W1,W2}/M_{W1,W2} \simeq 20\%$ at mass scales within the LHC reach, as shown in Fig. 2. The prediction of broad resonances is a distinctive feature of Higgsless models, and more generally extra-dimensional theories [69]. The benchmark model adopted for experimental analysis, described in [70], predicts instead a SM-like $W'^{\pm}$-boson purely decaying into fermion pairs. As a consequence, its width is generally expected to be very narrow. In this case, signal events are rather clustered towards the Jacobian peak in the transverse mass distribution, so that performing a simple counting experiment in that region often gives a signal-to-background ratio that is high enough for de-

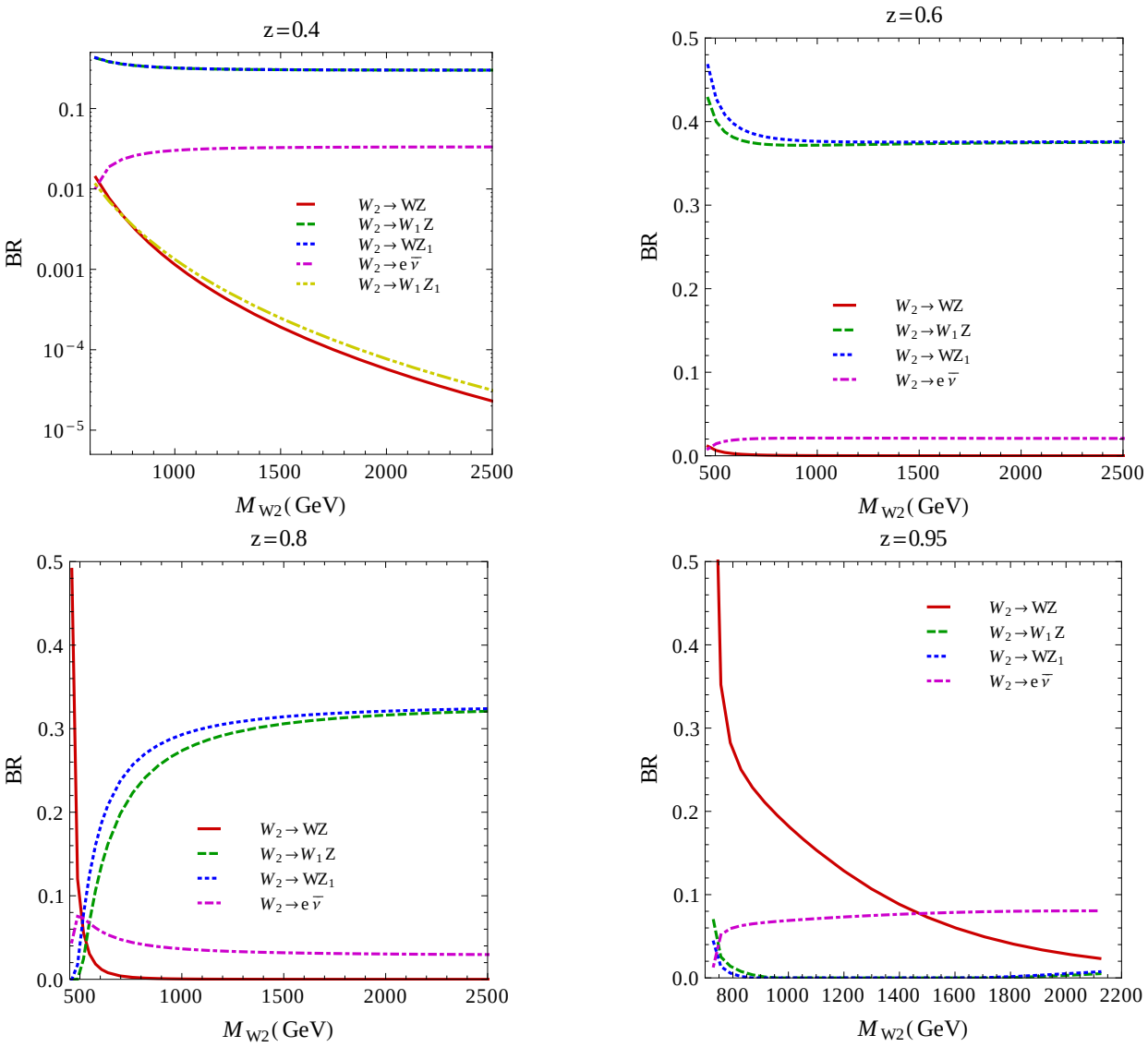

FIG. 3: W_2-boson branching ratios as a function of M_{W2} for z =0.4,0.6,0.8,0.95.

tection. Broad resonances are definitely more challenging to be analyzed than narrow ones. Signal events are indeed spread out over a wider area, not allowing a clear identification based on the shape. The question then becomes whether or not one can distinguish these events from the background or other non-resonant new physics such as contact interactions or any unshaped enhancement over the SM background.

Let us now discuss the $W^{\pm}_{1,2}$-boson branching ratios. The lighter extra gauge bosons, $W^{\pm}_1$ can decay only into SM fermion and gauge boson pairs: $W^{\pm}_1 \to ff'$ and $W^{\pm}_1 \to W^{\pm}Z$. For all z-values, the diboson channel is the dominant one, the fermion decay being suppressed by EWPT. The decay into electrons, is an increasing function of the z parameter, but is

always below 2%. However, it can compete with the diboson one if one chooses to rely on clean purely leptonic final states as $BR(W_1 \to WZ \to e\nu_e\mu^-\mu^+) \simeq BR(W_1 \to WZ)/300$. The $W_2^\pm$-boson BRs have a more complicated structure. They are displayed in Fig. 3 for four representative values of the z-parameter. The heavier charged extra gauge bosons are mainly axial, hence their decay into SM gauge boson pairs is highly suppressed. Their basic decay modes are into SM fermions and diboson pairs with at least one extra heavy gauge boson: $W_2^\pm \to ff', W_1^\pm Z, W^\pm Z_1, W_1^\pm Z_1$. As for the lighter extra gauge bosons, the dominant decay mode is the mixed diboson channel $W_2^\pm \to W_1^\pm Z, W^\pm Z_1$. The decay into electron neutrino pairs increases with z, never exceeding 10% level. But again, if one wants to rely on purely leptonic final states, bosonic and fermionic decay modes compete. For high z values, or almost degenerate scenario $M_{W1} \simeq M_{W2}$, the latter can even take over owing to the fact that the $W_2^\pm \to W_1^\pm Z, W^\pm Z_1$ modes are kinetically not allowed, as shown in the bottom-right panel of Fig. 3.

An exception to this trend appears in the low edge of the spectrum for high z values. In this case, the $W_2^\pm \to W_1^\pm Z, W^\pm Z_1$ channels are kinematically suppressed owing to the smallness of $\Delta M = M_{W2} - M_{W1}$, and the fermion channel is strongly constrained by EWPT. As a consequence, the only decay mode left is $W_2^\pm \to W^\pm Z$. This channel, a priory subdominant owing to the axial nature of the $W_2^\pm$-boson, becomes the leading one as shown in the bottom panels of Fig. 3, giving rise to an extremely narrow resonance.

IV. DRELL-YAN PRODUCTION AT THE LHC AND THE TEVATRON

Let us now consider the production of the four heavy extra gauge bosons, $W_{1,2}^\pm$, predicted by the 4-site Higgsless model at the LHC and the Tevatron through the Drell-Yan channel. In contrast with the existing fermiophobic Higgsless literature, quite large couplings between SM fermions and extra gauge bosons are indeed allowed by EWPT as discussed in the previous section.

In the following, we analyze in detail the two charged Drell-Yan processes:

$$pp \to W, W_{1,2} \to e\nu_e, \qquad p\bar{p} \to W, W_{1,2} \to e\nu_e \tag{3}$$

at the LHC and the Tevatron, respectively. The two channels differ only by the initial state, and are characterized by one isolated electron (or positron) in the final state plus missing

transverse momentum. In our notation, $e\nu_e$ indicates both $e\bar{\nu}_e$ and $e^+\nu_e$. These processes can involve the production of the four charged extra gauge bosons, $W^{\pm}_{1,2}$, as intermediate states. They are described by the generic formula

$$\mathrm{d}\sigma^{h_1h_2}(P_1,P_2,p_f) = \sum_{i,j}\int \mathrm{d}x_1\mathrm{d}x_2 \; f_{i,h_1}(x_1,Q^2) f_{j,h_2}(x_2,Q^2)\,\mathrm{d}\hat{\sigma}^{ij}(x_1P_1,x_2P_2,p_f), \qquad (4)$$

where p_f summarizes the final-state momenta, f_{i,h_1} and f_{j,h_2} are the distribution functions of the partons i and j in the incoming hadrons h_1 and h_2 with momenta P_1 and P_2, respectively, Q is the factorization scale, and $\hat{\sigma}^{ij}$ represent the cross sections for the partonic processes. At the LHC, since the two incoming hadrons are protons and we sum over final states with opposite charges, we find

$$\begin{aligned}\mathrm{d}\sigma^{h_1h_2}(P_1,P_2,p_f) = \int \mathrm{d}x_1\mathrm{d}x_2 \quad & \sum_{U=u,c}\sum_{D=d,s}\Big[f_{\bar{\mathrm{D}},\mathrm{p}}(x_1,Q^2) f_{\mathrm{U},\mathrm{p}}(x_2,Q^2)\,\mathrm{d}\hat{\sigma}^{\bar{\mathrm{D}}\mathrm{U}}(x_1P_1,x_2P_2,p_f) \\ & + f_{\bar{\mathrm{U}},\mathrm{p}}(x_1,Q^2) f_{\mathrm{D},\mathrm{p}}(x_2,Q^2)\,\mathrm{d}\hat{\sigma}^{\bar{\mathrm{U}}\mathrm{D}}(x_1P_1,x_2P_2,p_f) \\ & + f_{\mathrm{D},\mathrm{p}}(x_1,Q^2) f_{\bar{\mathrm{U}},\mathrm{p}}(x_2,Q^2)\,\mathrm{d}\hat{\sigma}^{\mathrm{D}\bar{\mathrm{U}}}(x_1P_1,x_2P_2,p_f) \\ & + f_{\mathrm{U},\mathrm{p}}(x_1,Q^2) f_{\bar{\mathrm{D}},\mathrm{p}}(x_2,Q^2)\,\mathrm{d}\hat{\sigma}^{\mathrm{U}\bar{\mathrm{D}}}(x_1P_1,x_2P_2,p_f)\Big]. \end{aligned} \qquad (5)$$

Analogously, at the proton-antiproton collider Tevatron we have:

$$\begin{aligned}\mathrm{d}\sigma^{h_1h_2}(P_1,P_2,p_f) = \int \mathrm{d}x_1\mathrm{d}x_2 \quad & \sum_{U=u,c}\sum_{D=d,s}\Big[f_{\bar{\mathrm{D}},\mathrm{p}}(x_1,Q^2) f_{\mathrm{U},\bar{\mathrm{p}}}(x_2,Q^2)\,\mathrm{d}\hat{\sigma}^{\bar{\mathrm{D}}\mathrm{U}}(x_1P_1,x_2P_2,p_f) \\ & + f_{\bar{\mathrm{U}},\mathrm{p}}(x_1,Q^2) f_{\mathrm{D},\bar{\mathrm{p}}}(x_2,Q^2)\,\mathrm{d}\hat{\sigma}^{\bar{\mathrm{U}}\mathrm{D}}(x_1P_1,x_2P_2,p_f) \\ & + f_{\mathrm{D},\mathrm{p}}(x_1,Q^2) f_{\bar{\mathrm{U}},\bar{\mathrm{p}}}(x_2,Q^2)\,\mathrm{d}\hat{\sigma}^{\mathrm{D}\bar{\mathrm{U}}}(x_1P_1,x_2P_2,p_f) \\ & + f_{\mathrm{U},\mathrm{p}}(x_1,Q^2) f_{\bar{\mathrm{D}},\bar{\mathrm{p}}}(x_2,Q^2)\,\mathrm{d}\hat{\sigma}^{\mathrm{U}\bar{\mathrm{D}}}(x_1P_1,x_2P_2,p_f)\Big]. \end{aligned} \qquad (6)$$

The tree-level amplitudes for the partonic processes have been generated by means of `PHACT` [71], a set of routines based on the helicity-amplitude formalism of Ref. [72]. The matrix elements have been inserted in the Monte Carlo event generator `FAST_2f`, dedicated to Drell-Yan processes at the EW and QCD leading order. `FAST_2f` can compute simultaneously new-physics signal and SM background. It can generate cross-sections and distributions for any observable, including any kind of kinematical cuts. The code is moreover interfaced with `PYTHIA` [73]. This feature can allow a more realistic analysis, once `FAST_2f` is matched with detector simulation programs.

A. Numerical setup

For the numerical results presented here, we have used the following input values [74]: $M_Z = 91.187\,\mathrm{GeV}$, $\Gamma_\mathrm{Z} = 2.512\,\mathrm{GeV}$, $\Gamma_\mathrm{W} = 2.105\,\mathrm{GeV}$, $\alpha(M_Z) = 1/128.88$, $G_F = 1.166 \times 10^{-5}\ \mathrm{GeV}^{-2}$. Additional input parameters are the quark-mixing matrix elements [75], whose values have been taken to be $|V_\mathrm{ud}| = |V_\mathrm{cs}| = 0.975$, $|V_\mathrm{us}| = |V_\mathrm{cd}| = 0.222$, and zero for all other relevant matrix elements. In our scheme, the weak mixing-angle and the W-boson mass are derived quantities. We use the fixed-width scheme for the matrix element evaluation, and the CTEQ6L[76] for the parton distribution functions at the factorization scale:

$$Q^2 = \frac{1}{2}\left(P_\mathrm{T}^2(e) + P_\mathrm{T}^2(\nu_e)\right) \tag{7}$$

where P_T denotes the transverse momentum. This scale choice appears to be appropriate for the calculation of differential cross sections, in particular for lepton distributions at high energy scales and is adapted from Ref.[77]. When considering the DY-channel at the LHC, we have moreover implemented the general set of acceptance cuts defined in [78] and here below summarized:

- electron (or positron) transverse momentum $P_\mathrm{T}(e) > 25\,\mathrm{GeV}$,
- missing transverse momentum $P_\mathrm{T}^\mathrm{miss} > 25\,\mathrm{GeV}$,
- electron (or positron) pseudo-rapidity $|\eta_e| < 2.1$,

where $\eta_e = -\log\left(\tan\theta_e/2\right)$, and θ_e is the polar angle of the charged lepton e with respect to the beam. For the analysis at the Tevatron, we include instead a global acceptance of 40% [58]. In both cases, we assume 100% efficiency on charged lepton reconstruction. Additional dedicated kinematical cuts will be described in due time.

For the LHC analysis, we present results at the present center-of-mass (c.o.m.) energy $\sqrt{s} = 7\,\mathrm{TeV}$ and two values of the integrated luminosity: $L = 1\,\mathrm{fb}^{-1}$ (nowadays) and $L = 10\,\mathrm{fb}^{-1}$ (1 year projection). We moreover give some hints for the LHC at its design c.o.m. energy $\sqrt{s} = 14\,\mathrm{TeV}$ and $L = 10\,\mathrm{fb}^{-1}$. For the Tevatron, we work within the actual setup: c.o.m. energy $\sqrt{s} = 1.96\,\mathrm{TeV}$ and $L = 10\,\mathrm{fb}^{-1}$.

	z	$M_{W1,W2}$(GeV)	$\Gamma_{W1,W2}$(GeV)	$a_{W1,W2}$
a	0.4	410,1000	3.5,24.8	-0.027,0.23
b	0.6	486,794	5.7,15.9	-0.052,0.18
c	0.8	518,636	5.4,2.6	-0.058,0.13
d	0.95	1019,1101	9.4,13.5	-0.062,0.26

TABLE I: Four representative scenarios for the 4-site Higgsless model.

B. $W^{\pm}_{1,2}$-boson production at the LHC and the Tevatron

In this section, we analyze the production of the four extra charged gauge bosons in Drell-Yan channel. We consider four representative cases of mass spectrum and couplings within the parameter space allowed by EWPT and unitarity bounds, as shown in Table I. These four examples give an idea of the possible scenarios predicted by the 4-site Higgsless model. In the model in fact the ratio between the masses of the first and second gauge boson triplet, i.e. $z = M_1/M_2$, is a free parameter. Hence, the distance between the two masses is arbitrary as well. We have thus chosen four cases, corresponding to z=0.4, 0.6, 0.8, 0.95, and representing from left to right very distant resonances, the flat-metric scenario, and a spectrum which tends to degeneracy by increasing z.

In order to illustrate spectrum and behaviors of the new heavy $W_{1,2}$ bosons, we have chosen to analyze the distribution in the transverse mass of the lepton pair, $M_t(e\nu_e)$, for the four scenarios of Tab. I. In Fig. 4, we plot the total number of events as a function of the dilepton transverse mass $M_t(e\nu_e)$ at the Tevatron and at the 7 TeV LHC with L=1 fb^{-1}. We sum over the charged conjugate processes and apply standard acceptance cuts. In most of the cases, one cannot identify the lighter resonance. This is a consequence of an intrinsic property of the model. That is, in most part of the parameter space, the axial spin-one W_2-boson is more strongly coupled to fermions than the vector spin-one W_1-boson. Thus, the 4-site model appears to be degenerate with popular theories predicting a single charged extra gauge boson, W'. As a consequence, the same experimental analysis performed for the single-resonant benchmark model in [70] could be directly applied to the 4-site Higgsless theory.

In order to estimate the detection rate expected at the Tevatron and the 7 TeV LHC

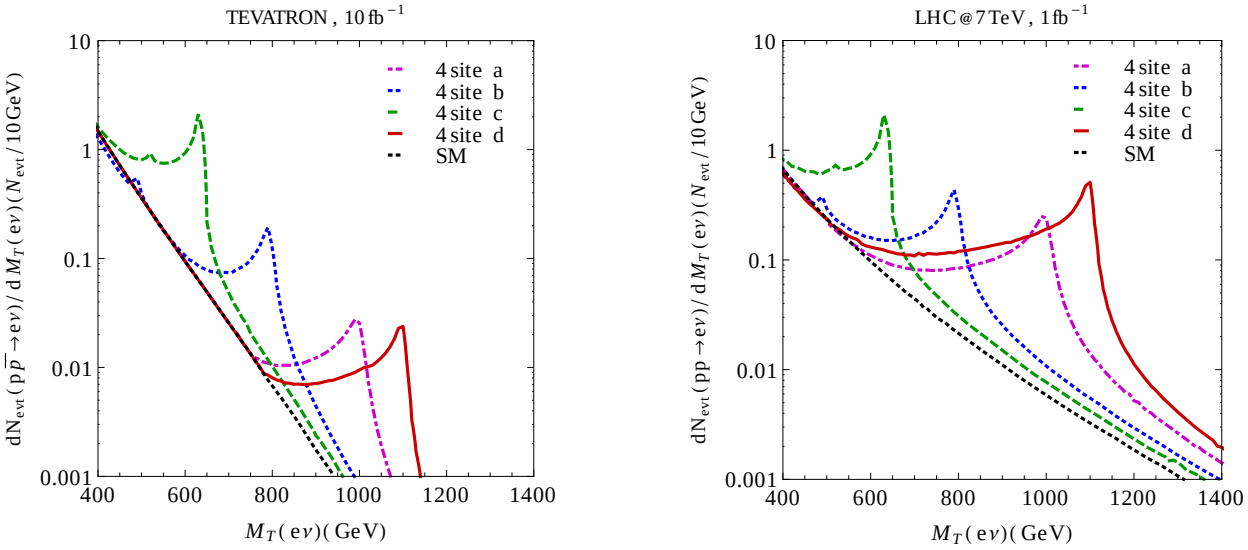

FIG. 4: Left: Total number of events in a 10 GeV-binning versus the lepton transverse mass, $M_t(e\nu_e)$, for the process $p\bar{p} \to e\nu_e$ at the Tevatron with integrated luminosity L=10 fb^{-1} for the four scenarios of Table I. We sum over charge conjugate channels. A global 40% acceptance is applied. Right: Same distributions for the process $pp \to e\nu_e$ at the 7 TeV LHC with integrated luminosity L=1 fb^{-1}. Standard acceptance cuts are applied.

for the Drell-Yan production of the extra $W^{\pm}_{1,2}$ gauge bosons, in Table II and we have listed number of SM background events, signal events and corresponding significance for the four scenarios given in Tab. I. We have superimposed the additional dedicated kinematical cut $M_t(e\nu_e) \geq M_t^{cut}$, where the value of M_t^{cut} is extracted from Fig. 4 by taking the point where the total number of events intersects the SM background. The Gaussian statistical significance is defined as $\sigma = \frac{N^T_{evt} - N^B_{evt}}{a}$, where $N^{T(B)}_{evt}$ is the number of total (background) events and a is $\sqrt{N^B_{evt}}$ if $N^B_{evt} > 1$ and 1 otherwise.

In order to enhance the signal-over-background ratio, the lower bound on the dilepton transverse mass, M_{cut}, must be indeed chosen *ad hoc*. In Fig. 5, we show how M_{cut} varies with M_{W1} for the four representative z-values in Tab. I. Left and right panels of Fig. 5 refer to the Tevatron and the 7 TeV LHC, respectively. We note that $M_{cut} > M_{W1}$ for $z \leq 0.5$. This means that the lighter resonances are in a region where the 4-site model predicts a depletion of events compared to the SM.

The corresponding total cross-sections integrated over the window, $M_T(e\nu_e) \geq M_{cut}$, are

	M_{cut}^{TEV} (GeV)	$N_{evt}^{TEV}(B)$	$N_{evt}^{TEV}(T-B)$	σ^{TEV}	M_{cut}^{LHC} (GeV)	$N_{evt}^{LHC}(B)$	$N_{evt}^{LHC}(T-B)$	σ^{LHC}
a	751	0.97	3	3	556	18	38	8.9
b	474	38	17	2.8	464	39	45	7.2
c	355	200	159	11.2	327	207	167	11.6
d	781	0.65	2.7	2.7	526	23	78	16.3

TABLE II: The first column represents the scenario as defined in Tab. I. The following first four columns give the lower bound on the dilepton transverse mass, the number of expected background events, the number of signal events and the corresponding statistical significance at the Tevatron with 10 fb^{-1}. The remaining four columns contain the same data for the LHC with 1 fb^{-1}.

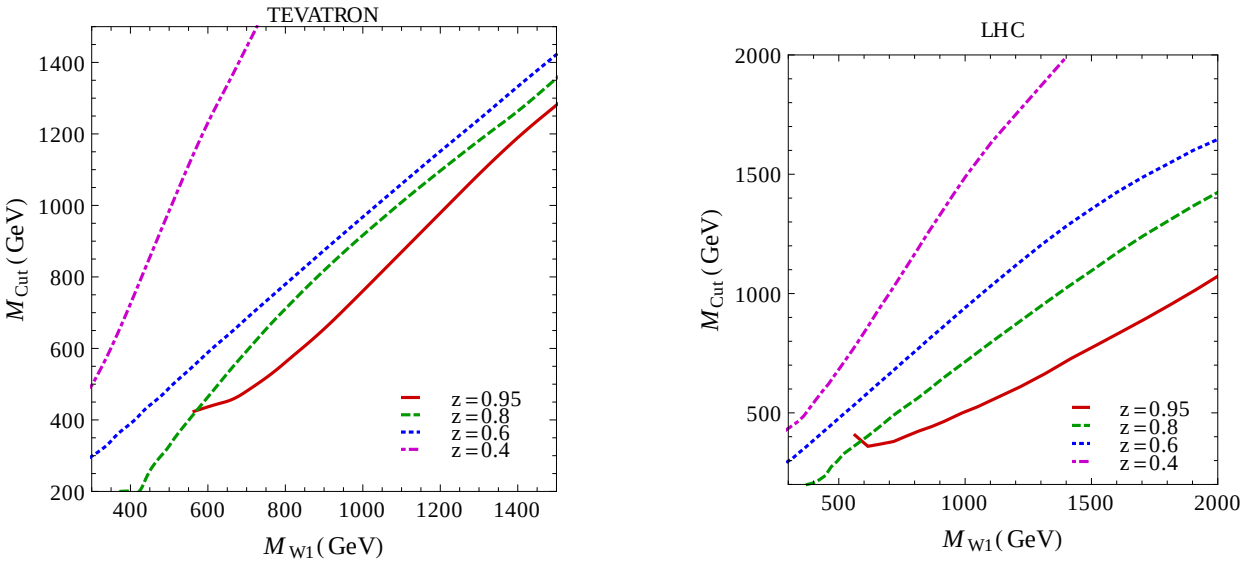

FIG. 5: Lower bound on the dilepton transverse mass, M_{cut}, as a function of the lighter extra gauge boson mass, M_{W1}, for four values of the free z-parameter: z=0.4, 0.6, 0.8, 0.95. At Tevatron (left) and LHC (right)

shown in Fig. 6 for the Tevatron and Fig. 7 for the 7 TeV LHC as a function of M_{W1}. We consider the usual four z-values: z=0.4, 0.6, 0.8, 0.95. These are just bare values, useful only to give an idea of the magnitude of the expected cross-sections around the resonances. The displayed cross-sections have been indeed calculated for the maximum value of the W_1-boson coupling to electrons, a_{W1}, allowed by EWPT at fixed z.

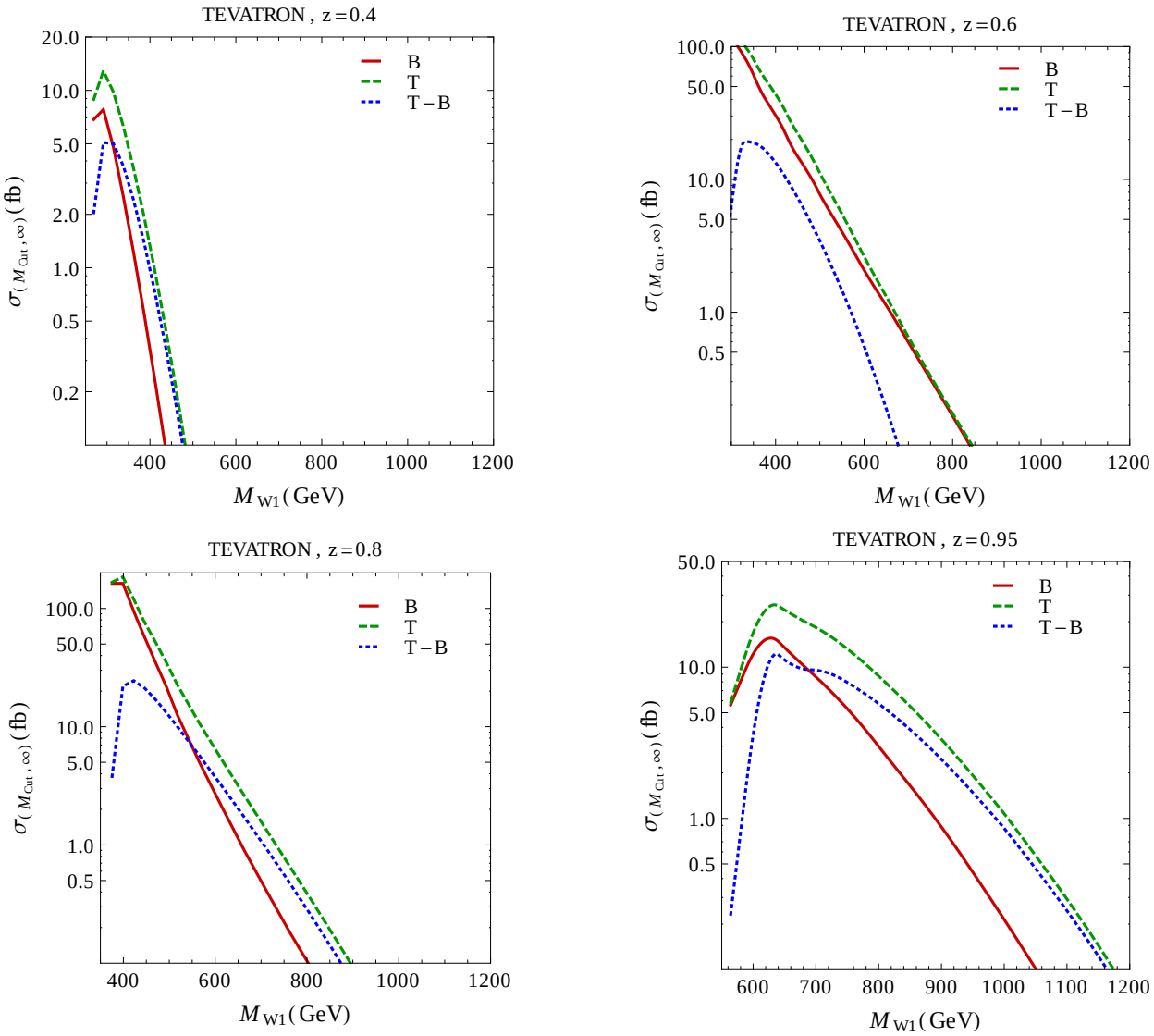

FIG. 6: $W^{\pm}_{1,2}$-boson cross-sections, for the maximal a_{W1} coupling allowed by EWPT, integrated over the mass window $M_T(e\nu_e) \geq M_{cut}$, as function of M_{W1} at the Tevatron. The dashed line represents the total cross-section (T), including the interference between $W_{1,2}$-boson signal and SM background. The solid line shows the SM background (B). The dotted line corresponds to their difference: S=T-B. In the four plots, the free z-parameter assumes the values: z=0.4, 0.6, 0.8, 0.95.

At fixed mass, M_{W1}, the cross-section gets larger by increasing the value of the z-parameter. This effect is due to the fact that high z-values help in relaxing the EWPT constraints on the $W_{1,2}$-boson coupling to SM fermions, as previously shown in Fig. 1. The signal cross section at the Tevatron can thus lie in the range: 5 fb $\leq \sigma_{T-B} \leq$ 25 fb for the

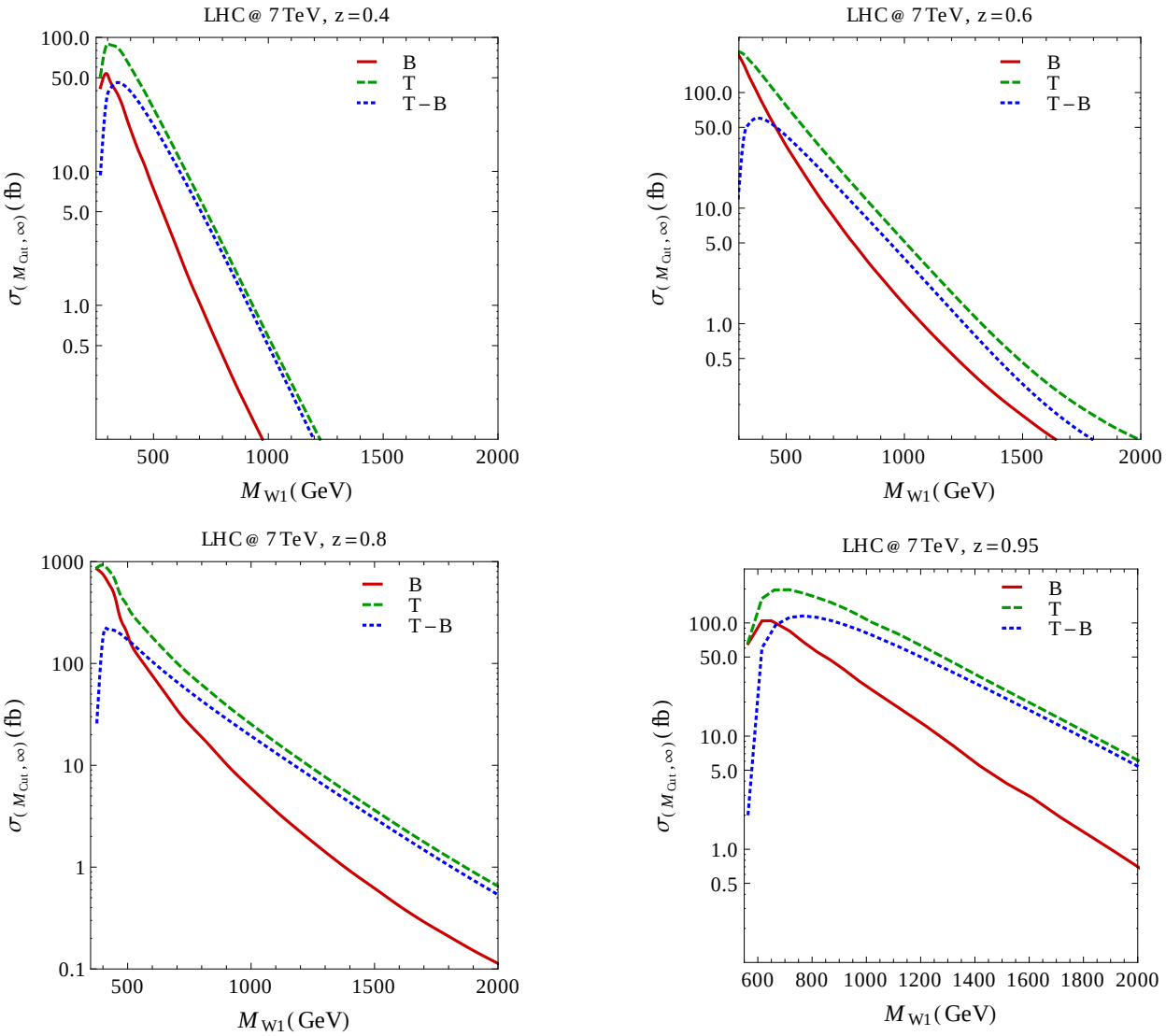

FIG. 7: $W^{\pm}_{1,2}$-boson cross-sections, for the maximal a_{W1} coupling allowed by EWPT, integrated over the mass window $M_T(e\nu_e) \geq M_{cut}$, as function of M_{W1} at the 7 TeV LHC. The dashed line represents the total cross-section (T), including the interference between $W_{1,2}$-boson signal and SM background. The solid line shows the SM background (B). The dotted line corresponds to their difference: S=T-B. In the four plots, the free z-parameter assumes the values: z=0.4, 0.6, 0.8, 0.95.

W_1-boson mass interval allowed by EWPT and unitarity. At the 7 TeV LHC, the expected cross section increases by about an order of magnitude, reaching values of a few hundred fb.

V. $W^{\pm}_{1,2}$ EXCLUSION AND DISCOVERY REACH AT THE TEVATRON AND LHC

In this section, we discuss the prospects of discovering the four charged spin-1 bosons predicted by the 4-site Higgsless model at the LHC. Let us start by deriving the present exclusion limits on the $W_{1,2}$-bosons from the Tevatron experiment. We consider both neutral and charged Drell-Yan channels, $p\bar{p} \to e^- e^+$ and $p\bar{p} \to e\nu_e$, at the collected luminosity L=10 fb^{-1}, and we include a global 40% acceptance and efficiency factor. For the neutral Drell-Yan channel, we compute the expected number of events in the asymmetrical mass window $M_{inv}(e^+e) \geq M_{Z1} - 3R_{TEV}$, where $R_{TEV} \simeq 3.4\% M$ is the approximated D0 mass resolution (see [47] and references therein). For the charged Drell-Yan channel instead, we consider the mass window: $M_t(e\nu_e) \geq M_{cut}$ as previously discussed. For both processes, we then evaluate the region of the parameter space where the Gaussian statistical significance is bigger than 2: $\sigma = \frac{N^T_{evt} - N^B_{evt}}{a} \geq 2$, where $N^{T(B)}_{evt}$ is the number of total (SM background) events and $a = \sqrt{N^B_{evt}}$ if $N^B_{evt} > 1$ and $a = 1$ otherwise. The expected 95% CL exclusion region in the plane M_{W1}, a_{W1} is depicted in Fig. 8 by the black shaded area. The 4-site model can be constrained by present data like other popular W' theories. Assuming maximal values for the $W_{1,2}$-boson couplings to SM fermions, the direct limit on the mass of the heavy extra resonances is indeed $M_{W1} \geq 1100$ GeV for z=0.95 as displayed in the bottom-right panel of Fig. 8. For z=0.4 on the other hand, the mass bound is about $M_{W1} \geq 400$ GeV as shown in the top-left panel of Fig.8. This is not surprising as the corresponding bound on M_{W2} would be 1 TeV as above, and the lighter resonance would actually be invisible. These limits mainly come from the neutral Drell-Yan channel, which might involve the production and decay of the two neutral extra gauge bosons, $Z_{1,2}$, predicted by the 4-site model (see [47, 49, 50]). Here, they have been appropriately converted in order to appear in the parameter space expressed in terms of the charged M_{W1}, a_{W1} physical observables.

In the same Fig.8, we also show the 95% CL exclusion limits that one could derive at different stages of the LHC. These contour plots have been computed by integrating the cross section in the domain $M_t(e\nu_e) \geq M_{cut}$, and assuming the acceptance times efficiency setup described in Sec. IV A. The cyan shaded area in Fig.8 shows the 95% CL exclusion limits on $W_{1,2}$-boson mass and coupling that one could extract from present data at the 7 TeV LHC, which has now collected over 1 fb^{-1}. As one can see the LHC greatly extends the

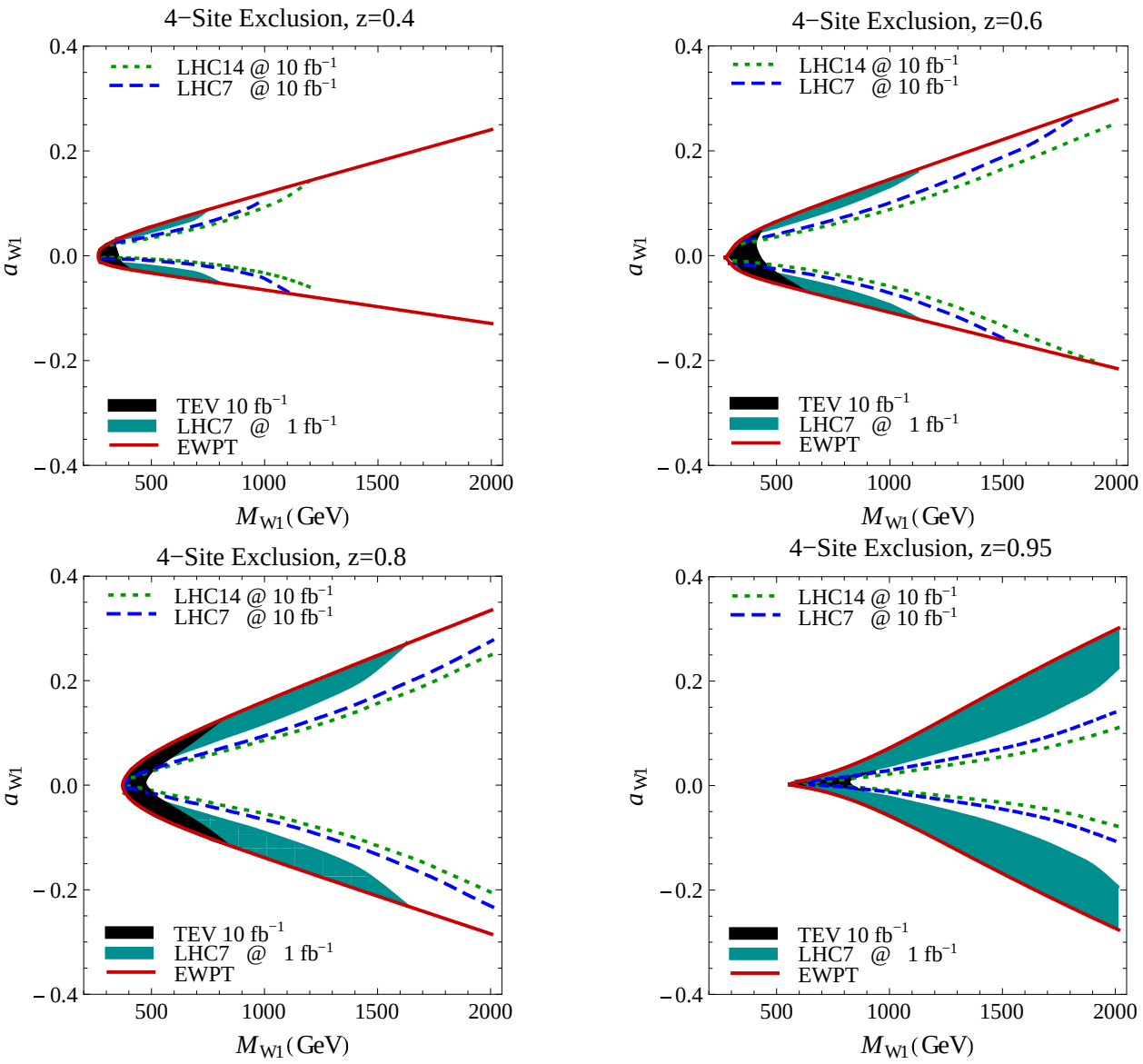

FIG. 8: 95% CL exclusion limits in the (M_{W1}, a_{W1}) plane at the 7 TeV LHC with an integrated luminosity of 10 fb^{-1} (blue dashed line), and at the 14 TeV LHC with 10 fb^{-1} (dotted green line). The red solid contour defines the parameter space allowed by EWPT and unitarity. The black shaded region represents the 95% CL exclusion limits from direct searches in the Drell-Yan channel at the Tevatron with L=10 fb^{-1}. The cyan shaded region gives the expected 95% CL exclusion limits at the actual 7 TeV LHC with L=1 fb^{-1}. From top-left to bottom-right, the z-parameter is fixed to be: $z = 0.4$, 0.6, 0.8 and 0.95.

Tevatron bounds, being able to exclude the entire mass spectrum in the almost degenerate scenario not only for maximal couplings. We furthermore compare this result with the 95% CL exclusion limit one could reach in one year from now, that is at the 7 TeV LHC with an

expected integrated luminosity L=10 fb^{-1}. In this second stage, the LHC could exclude the 4-site model up to energy scales of the order of $M_{W1} \geq 1100$, 1800, 2000 GeV for maximal $a_{W1,W2}$ couplings allowed by EWPT and z=0.4, 0.6, 0.8 (or 0.95) respectively. Finally, we analyze the energy dependence of such limits, displaying the 95% CL exclusion limits at the project 14 TeV LHC with L=10 fb^{-1}. This upgrade would further extend the exclusion potential by a few hundreds of GeV. For high-intermediate values of the free z-parameter, a sizeable portion of the parameter space could be analyzed and perhaps excluded. The low z range would need higher energy and luminosity.

In Fig. 9, we show the prospects of discovering the four charged spin-1 bosons predicted by the 4-site Higgsless model during the LHC early and future stages, as done above for the exclusion (now simply requiring $\sigma \geq 5$).

The dashed blue line gives the 5σ-discovery potential in the next one-year period at the 7 TeV LHC with L=10 fb^{-1}. The dotted green line projects the discovery reach at the 14 TeV LHC with L=10 fb^{-1}. As for the exclusion, the discovery contour plots have been obtained by integrating the cross section over the domain $M_t(e\nu_e) \geq M_{cut}$, and assuming the acceptance times efficiency setup described in Sec. IV A. The global discovery reach during the early run of the LHC is substantial. The charged extra gauge bosons could be detected up to $M_{W1} \sim$ 1000, 1300, 2000 GeV for z = 0.4, 0.6, 0.8 (or 0.95) respectively.

To conclude, we show in Fig. 10 the minimum luminosity needed to claim a $W_{1,2}$-boson discovery during the early stage (left panel) and project stage (right panel) of the LHC.

VI. CONCLUSIONS

In this paper, we have studied the phenomenology of the next-to-minimal (or 4-site) Higgsless model, which extends the minimal (or 3-site) Higgsless model by including one additional site in the linear moose picture. The 4-site model is a deconstructed theory based on the $SU(2)_L \times SU(2)_1 \times SU(2)_2 \times U(1)_Y$ gauge symmetry. It predicts four charged and two neutral extra gauge bosons: $W^{\pm}_{1,2}$ and $Z_{1,2}$. We have focused on the properties of the charged gauge sector and on its discovery prospects at the 7 TeV LHC in the final state with one isolated electron (or positron) and large missing energy during the next year.

The phenomenology of the 4-site model is controlled by three free parameters beyond the SM ones: the two extra gauge boson masses, $M_{W1,W2}$ and the coupling between the

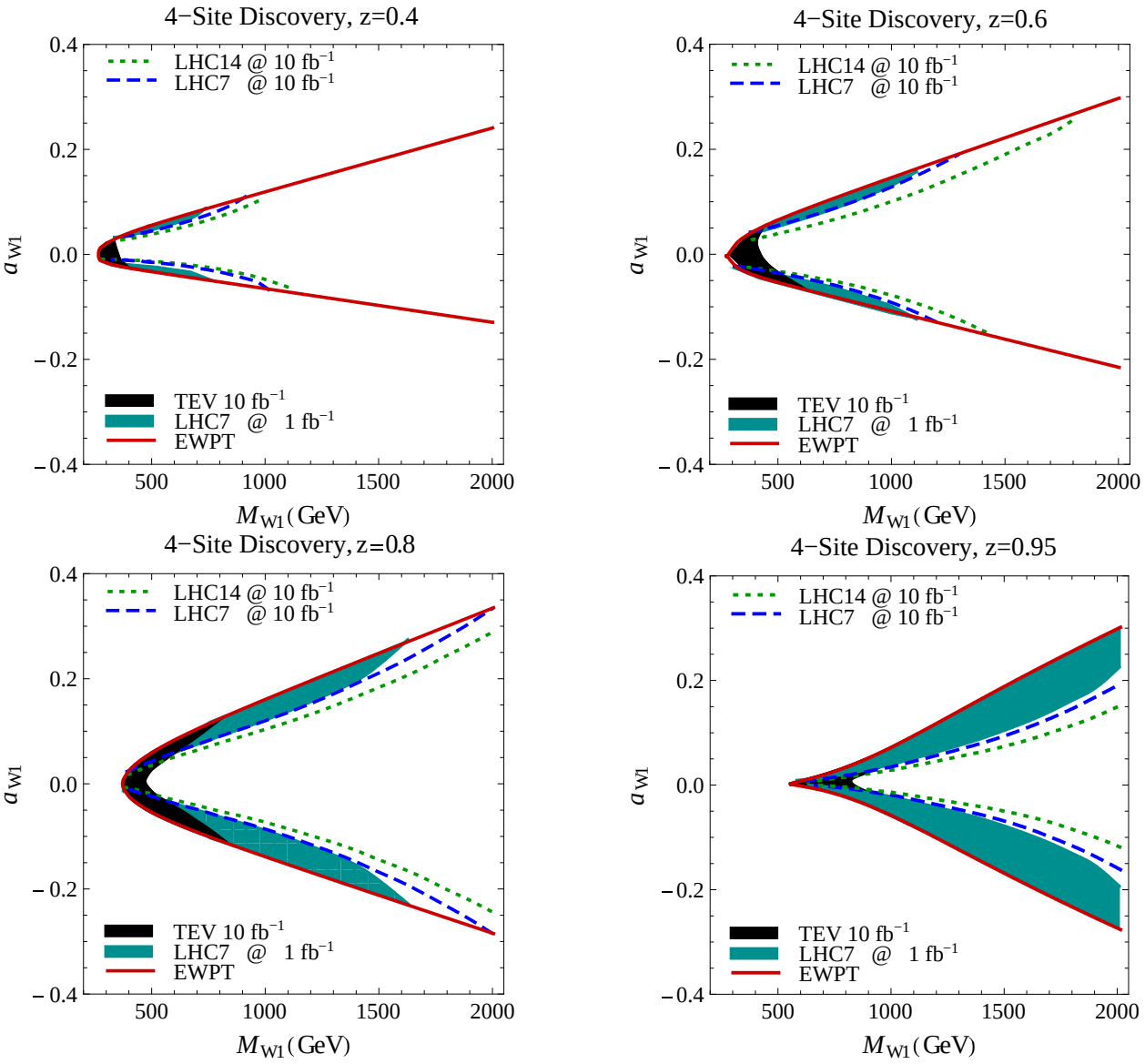

FIG. 9: $W_{1,2}$-boson discovery in the (M_{W1}, a_{W1}) plane at the 7 TeV LHC with an integrated luminosity L=10 fb^{-1} (blue dashed line), and at the 14 TeV LHC with 10 fb^{-1} (dotted green line). The red solid contour defines the parameter space allowed by EWPT and unitarity. The cyan shaded region gives the expected 95% CL exclusion limits at the actual 7 TeV LHC with L=1 fb^{-1}. From top-left to bottom-right, the z-parameter is fixed to be: $z = 0.4$, 0.6, 0.8 and 0.95.

lighter extra gauge boson and SM fermions, a_{W1}. At fixed ratio $z = M_1/M_2 \simeq M_{W1}/M_{W2}$, the model can be thus visualized in the (M_{W1}, a_{W1}) plane. The mass spectrum is bounded from above by the requirement of perturbative unitarity, and from below by EWPT. The viable mass range is thus around [250, 3000] GeV. EWPT also constrain the magnitude of the couplings. Nevertheless, the allowed parameter space is sizeable. This represents the

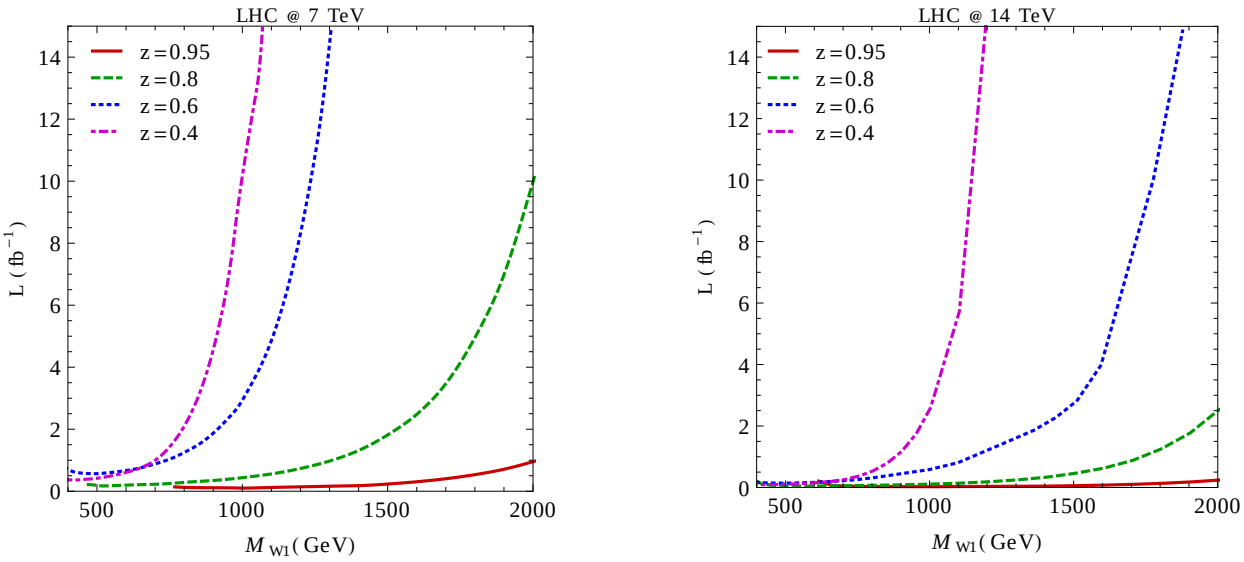

FIG. 10: Left: Minimum luminosity needed for a 5σ-discovery of $W_{1,2}$-bosons at the 7 TeV LHC, assuming maximal $W_{1,2}$-boson couplings to SM fermions and z=0.4, 0.6, 0.8, 0.95. Right: same curves at the upgraded 14 TeV LHC.

major novelty of the 4-site model which, in contrast to its minimal version (or three site model), can solve the dichotomy between unitarity and EWPT bounds without imposing the extra vector bosons to be fermiophobic. As a consequence, the Drell-Yan process becomes a relevant channel for the direct search of extra gauge bosons at the LHC.

In this paper, we have first described the main properties of the new $W_{1,2}$-bosons. We have shown their total decay widths and branching ratios into fermions and bosons. The results can be summarized in two main points. First, BRs into lepton pairs and boson pairs decaying in turn into leptons can compete when looking at purely leptonic final states. Within the 4-site Higgsless model, the DY process is thus a strong discovery channel. Second, in contrast to common W' bosons which purely decay into SM fermions and appear as narrow resonances, the $W_{1,2}$ bosons can display a broad peaking structure. This feature poses one more challenge to the experimental analyses commonly based on the assumption of narrow resonances.

In order to show what signature might be expected, we have presented four sample scenarios corresponding to different points in the parameter space. In the 4-site model, no relation between lighter and heavier extra gauge bosons is predicted ($z = M_1/M_2$ is a free parameter). So, for sake of completeness, we have chosen four cases where in principle the two $W_{1,2}$-bosons could appear as resonances either quite distant in mass or almost degenerate.

We have then computed the limits on $W_{1,2}$-boson masses and couplings from direct searches in both neutral and charged Drell-Yan channels at the Tevatron with integrated luminosity L=10 fb^{-1}. The outcome is that the 4-site model is weakly bounded. For low z values, only a small corner around the minimum mass, $M_{W1} \geq 350$ GeV, is excluded. For high z values, one can exclude the model up to $M_{W1} \simeq 1100$ GeV assuming maximal couplings between extra gauge bosons and SM fermions. The present data collected at the LHC, which has now over 1 fb^{-1}, extend the Tevatron limits by several hundreds of GeV. In the low edge of the z interval, the exclusion limit can reach $M_{W1} \simeq 800$ GeV. It further grows with increasing z, and can even exclude the entire mass spectrum in the almost degenerate scenario (z=0.95), not only for maximal couplings.

Looking at one-year timescale, we have shown how the expected 7 TeV LHC with L=10 fb^1 could sensibly extend the 4-site physics search to regions of the parameter space with smaller $W_{1,2}$-boson couplings to ordinary matter. The presented results are of course preliminary, coming from a pure parton level analysis. They nevertheless show that the 4-site model can be tested already during the early LHC stage in a large portion of its parameter space.

Note added in proof. Soon after the publication of our paper, the new results on the search for a new heavy gauge boson W' decaying to a charged lepton (muon or electron) and a neutrino at the LHC were published by the CMS experiment [79]. The experimental analysis is based on the data collected in 2011, which correspond to an integrated luminosity of 1.1 fb-1. As both setup and signal definition are different, we cannot directly compare the results of our paper with the limit placed by CMS.

Acknowledgments

E.A. and D.B. acknowledge financial support from the NExT Institute and SEPnet. E.A. thanks the theoretical physics department of the University of Torino for hospitality. The work of S.D.C., D.D. and L.F. is partly supported by the Italian Ministero dell'Istruzione, dell' Università e della Ricerca Scientifica, under the COFIN program (PRIN 2008).

[1] J. C. Pati and A. Salam, Phys. Rev. **D10**, 275 (1974).

[2] R. N. Mohapatra, J. C. Pati, and L. Wolfenstein, Phys. Rev. **D11**, 3319 (1975).

[3] G. Senjanovic and R. N. Mohapatra, Phys. Rev. **D12**, 1502 (1975).

[4] S. Gopalakrishna, T. Han, I. Lewis, Z.-g. Si, and Y.-F. Zhou, Phys.Rev. **D82**, 115020 (2010), 1008.3508.

[5] M. Frank, A. Hayreter, and I. Turan, Phys.Rev. **D83**, 035001 (2011), 1010.5809.

[6] A. Maiezza, M. Nemevsek, F. Nesti, and G. Senjanovic, Phys.Rev. **D82**, 055022 (2010), 1005.5160.

[7] M. Nemevsek, F. Nesti, G. Senjanovic, and Y. Zhang, Phys.Rev. **D83**, 115014 (2011), 1103.1627.

[8] J. R. Andersen et al. (2011), 1104.1255.

[9] F. Sannino, Acta Phys. Polon. **B40**, 3533 (2009), 0911.0931.

[10] J. R. Andersen, T. Hapola, and F. Sannino (2011), * Temporary entry *, 1105.1433.

[11] A. Belyaev et al., Phys. Rev. **D79**, 035006 (2009), 0809.0793.

[12] N. Arkani-Hamed, S. Dimopoulos, and G. R. Dvali, Phys. Lett. **B429**, 263 (1998), hep-ph/9803315.

[13] I. Antoniadis, N. Arkani-Hamed, S. Dimopoulos, and G. R. Dvali, Phys. Lett. **B436**, 257 (1998), hep-ph/9804398.

[14] L. Randall and R. Sundrum, Phys. Rev. Lett. **83**, 3370 (1999), hep-ph/9905221.

[15] C. Csaki, C. Grojean, H. Murayama, L. Pilo, and J. Terning, Phys. Rev. **D69**, 055006 (2004), hep-ph/0305237.

[16] K. Agashe, A. Delgado, M. J. May, and R. Sundrum, JHEP **08**, 050 (2003), hep-ph/0308036.

[17] C. Csaki, C. Grojean, L. Pilo, and J. Terning, Phys. Rev. Lett. **92**, 101802 (2004), hep-ph/0308038.

[18] R. Barbieri, A. Pomarol, and R. Rattazzi, Phys. Lett. **B591**, 141 (2004), hep-ph/0310285.

[19] Y. Nomura, JHEP **11**, 050 (2003), hep-ph/0309189.

[20] G. Cacciapaglia, C. Csaki, C. Grojean, and J. Terning, Phys. Rev. **D70**, 075014 (2004), hep-ph/0401160.

[21] G. Cacciapaglia, C. Csaki, C. Grojean, and J. Terning, Phys. Rev. **D71**, 035015 (2005), hep-ph/0409126.

[22] R. Contino, T. Kramer, M. Son, and R. Sundrum, JHEP **05**, 074 (2007), hep-ph/0612180.

[23] E. Accomando, I. Antoniadis, and K. Benakli, Nucl. Phys. **B579**, 3 (2000), hep-ph/9912287.

[24] E. E. Boos, M. A. Perfilov, M. N. Smolyakov, and I. P. Volobuev (2011), 1106.2400.

[25] K. Agashe, H. Davoudiasl, S. Gopalakrishna, T. Han, G.-Y. Huang, et al., Phys.Rev. **D76**, 115015 (2007), 0709.0007.

[26] K. Agashe, S. Gopalakrishna, T. Han, G.-Y. Huang, and A. Soni, Phys.Rev. **D80**, 075007 (2009), 0810.1497.

[27] N. Arkani-Hamed, A. G. Cohen, and H. Georgi, Phys. Rev. Lett. **86**, 4757 (2001), hep-th/0104005.

[28] N. Arkani-Hamed, A. G. Cohen, and H. Georgi, Phys. Lett. **B513**, 232 (2001), hep-ph/0105239.

[29] C. T. Hill, S. Pokorski, and J. Wang, Phys. Rev. **D64**, 105005 (2001), hep-th/0104035.

[30] H.-C. Cheng, C. T. Hill, S. Pokorski, and J. Wang, Phys. Rev. **D64**, 065007 (2001), hep-th/0104179.

[31] H. Abe, T. Kobayashi, N. Maru, and K. Yoshioka, Phys. Rev. **D67**, 045019 (2003), hep-ph/0205344.

[32] A. Falkowski and H. D. Kim, JHEP **08**, 052 (2002), hep-ph/0208058.

[33] L. Randall, Y. Shadmi, and N. Weiner, JHEP **01**, 055 (2003), hep-th/0208120.

[34] D. T. Son and M. A. Stephanov, Phys. Rev. **D69**, 065020 (2004), hep-ph/0304182.

[35] J. de Blas, A. Falkowski, M. Perez-Victoria, and S. Pokorski, JHEP **08**, 061 (2006), hep-th/0605150.

[36] R. Casalbuoni, S. De Curtis, D. Dolce, and D. Dominici, Phys. Rev. **D71**, 075015 (2005), hep-ph/0502209.

[37] R. S. Chivukula, E. H. Simmons, H.-J. He, M. Kurachi, and M. Tanabashi, Phys. Rev. **D72**, 075012 (2005), hep-ph/0508147.

[38] R. Sekhar Chivukula, E. H. Simmons, H.-J. He, M. Kurachi, and M. Tanabashi, Phys. Rev. **D72**, 095013 (2005), hep-ph/0509110.

[39] J. Bechi, R. Casalbuoni, S. De Curtis, and D. Dominici, Phys. Rev. **D74**, 095002 (2006), hep-ph/0607314.

[40] R. Casalbuoni, S. De Curtis, D. Dominici, and D. Dolce, JHEP **08**, 053 (2007), arXiv:0705.2510 [hep-ph].

[41] A. Birkedal, K. Matchev, and M. Perelstein, Phys. Rev. Lett. **94**, 191803 (2005), hep-ph/0412278.

[42] A. Belyaev (2007), 0711.1919.

[43] H.-J. He et al., Phys. Rev. **D78**, 031701 (2008), 0708.2588.

[44] T. Abe, S. Matsuzaki, and M. Tanabashi, Phys. Rev. **D78**, 055020 (2008), 0807.2298.

[45] T. Ohl and C. Speckner, Phys.Rev. **D78**, 095008 (2008), 0809.0023.

[46] T. Abe, T. Masubuchi, S. Asai, and J. Tanaka (2011), * Temporary entry *, 1103.3579.

[47] E. Accomando, S. De Curtis, D. Dominici, and L. Fedeli, Phys. Rev. **D79**, 055020 (2009), 0807.5051.

[48] E. Accomando, D. Becciolini, S. De Curtis, D. Dominici, and L. Fedeli (2011), * Temporary entry *, 1105.3896.

[49] E. Accomando, S. De Curtis, D. Dominici, and L. Fedeli, Phys.Rev. **D83**, 015012 (2011), 1010.0171.

[50] E. Accomando, S. De Curtis, D. Dominici, and L. Fedeli, Nuovo Cim. **123B**, 809 (2008), 0807.2951.

[51] E. Accomando, A. Belyaev, L. Fedeli, S. F. King, and C. Shepherd-Themistocleous, Phys.Rev. **D83**, 075012 (2011), 1010.6058.

[52] O. Cata, G. Isidori, and J. F. Kamenik, Nucl. Phys. **B822**, 230 (2009), 0905.0490.

[53] S. Matsuzaki, R. S. Chivukula, E. H. Simmons, and M. Tanabashi, Phys. Rev. **D75**, 073002 (2007), hep-ph/0607191.

[54] R. S. Chivukula, E. H. Simmons, H.-J. He, M. Kurachi, and M. Tanabashi, Phys. Rev. **D71**, 115001 (2005), hep-ph/0502162.

[55] R. Sekhar Chivukula et al., Phys. Rev. **D74**, 075011 (2006), hep-ph/0607124.

[56] R. S. Chivukula, E. H. Simmons, S. Matsuzaki, and M. Tanabashi, Phys. Rev. **D75**, 075012 (2007), hep-ph/0702218.

[57] T. Aaltonen et al. (CDF Collaboration), Phys.Rev. **D83**, 031102 (2011), 1012.5145.

[58] V. M. Abazov et al. (D0 Collaboration), Phys.Lett. **B695**, 88 (2011), 1008.2023.

[59] S. Chatrchyan et al. (CMS Collaboration) (2011), * Temporary entry *, 1103.0981.

[60] S. Chatrchyan et al. (CMS Collaboration) (2011), * Temporary entry *, 1103.0030.

[61] R. S. Chivukula et al., Phys. Rev. **D74**, 075011 (2006), hep-ph/0607124.

[62] R. Casalbuoni, S. De Curtis, D. Dominici, and R. Gatto, Phys. Lett. **B155**, 95 (1985).

[63] R. Casalbuoni, S. De Curtis, D. Dominici, and R. Gatto, Nucl. Phys. **B282**, 235 (1987).

[64] M. E. Peskin and T. Takeuchi, Phys. Rev. Lett. **65**, 964 (1990).

[65] M. E. Peskin and T. Takeuchi, Phys. Rev. **D46**, 381 (1992).

[66] G. Altarelli and R. Barbieri, Phys. Lett. **B253**, 161 (1991).

[67] G. Altarelli, R. Barbieri, and F. Caravaglios, Int. J. Mod. Phys. **A13**, 1031 (1998), hep-ph/9712368.

[68] J. Alcaraz et al. (ALEPH Collaboration, DELPHI Collaboration, L3 Collaboration, OPAL Collaboration, LEP Electroweak Working Group) (2006), hep-ex/0612034.

[69] R. Kelley, L. Randall, and B. Shuve, JHEP **1102**, 014 (2011), 1011.0728.

[70] G. Altarelli, B. Mele, and M. Ruiz-Altaba, Z.Phys. **C45**, 109 (1989).

[71] A. Ballestrero (1999), hep-ph/9911318.

[72] A. Ballestrero and E. Maina, Phys. Lett. **B350**, 225 (1995), hep-ph/9403244.

[73] T. Sjostrand, S. Mrenna, and P. Skands, JHEP **05**, 026 (2006), hep-ph/0603175.

[74] W. M. Yao et al. (Particle Data Group), J. Phys. **G33**, 1 (2006).

[75] A. Hocker, H. Lacker, S. Laplace, and F. Le Diberder, Eur. Phys. J. **C21**, 225 (2001), hep-ph/0104062.

[76] J. Pumplin et al., JHEP **07**, 012 (2002), hep-ph/0201195.

[77] L. J. Dixon, Z. Kunszt, and A. Signer, Phys. Rev. **D60**, 114037 (1999), hep-ph/9907305.

[78] V. Abazov et al. (D0 Collaboration), Phys.Rev.Lett. **100**, 031804 (2008), 0710.2966.

[79] CMS PAS EXO-11-024 (2011), URL `http://cdsweb.cern.ch/search?cc=CMS+Physics+Analysis+Summari`